Signal Processing 134 (2017) 224–233

Contents lists available at ScienceDirect

Signal Processing

journal homepage: www.elsevier.com/locate/sigpro

Active contours driven by region-scalable fitting and optimized Laplacian of Gaussian energy for image segmentation

Keyan Ding[a], Linfang Xiao[b], Guirong Weng[a,*]

[a] School of Mechanical and Electric Engineering, Soochow University, Suzhou 215021, China
[b] College of Biosystems Engineering and Food Science, Zhejiang University, Hangzhou 310058, China

ARTICLE INFO

Keywords:
Image segmentation
Active contours
Level set method
Region-scalable fitting
Laplacian of Gaussian

ABSTRACT

It had been known that the famous region scalable-fitting model can segment the images with intensity inhomogeneity effectively, but it largely depends on the position of initial contour. In this paper, an active contour model which combines region-scalable fitting energy and optimized Laplacian of Gaussian (LoG) energy is proposed for image segmentation. We first present a LoG energy term optimized by an energy functional which can smooth the homogeneous regions and enhance edge information at the same time. Then, we integrate the optimized LoG energy term with the region-scalable fitting energy term which makes use of local region information to drive the curve towards the boundaries. With the addition of LoG term, the proposed model is insensitive to the positions of initial contour and realizes an accurate segmentation result. Experiments on some synthetic and real images have proved that the proposed model not only has a good robustness of initialization, but also has a higher segmentation accuracy and efficiency than other major region-based models.

1. Introduction

Image segmentation is a fundamental problem in the field of image processing and computer vision. In the past decades, a wide variety of image segmentation methods have been proposed. They can be divided into many categories: threshold-based methods, such as Otsu algorithm [1]; edge-based methods, including various edge detection operators [2]; region-based methods, for example, the region grow algorithm [3]; energy functional-based methods, such as active contour model [4]; specific theory-based methods, for example, the segmentation methods based on deep learning are often applied in boundary detection under the complicated background [5,6]. Active contour models (ACMs) have been widely applied in image segmentation since the presentation by Kass et al. [7]. The basic idea of ACM is to evolve a curve to extract the desired object based on an energy-minimizing method. They can achieve sub-pixel accuracy of target boundaries and obtain a smooth and closed contour. However, take traditional Snake model for example, it can easily converge to incorrect solutions due to the weak constraints. And they are not optimal for locating objects which have a known shape. Cootes et al. [7] proposed an active shape model (ASM) based on statistical shape analysis. It can locate the internal shape of objects, and the algorithm is simple and fast. Then Cootes et al. [8] proposed an active appearance model (AAM) based on ASM. ASM and AAM use the same underlying statistical model of the shape of objects, represent the shape by a set of landmark points and learn the ranges of shape variation from training images. ASM only utilizes the image texture in the neighbouring region of each landmark point, whereas AAM uses the appearance of the whole image region [9]. Thus, AAM gives a better match to the texture. In addition, in order to better estimate the pose of object, point set registration-based methods [10] are widely used in feature-based image registration.

In this study, we focus on implicit active contour models, namely active contour models in a level set formulation. The basic idea is that an active contour is implicitly represented as the zero level set of a function in a higher dimension (called level set function), and then the level set function is deformed according to an evolution equation [11]. Existing active contour models can be roughly categorized into two basic classes: *edge-based* models [12–17] and *region-based* models [18–28,31]. Edge-based models often use an edge indicator to attract the curve towards the target boundaries. They have been successfully used to extract the edges of a large gradient, but it is difficult to detect edges without obvious gradient, such as very smooth or discontinuous boundaries. Region-based models usually use a certain region descriptor to find a partition on the image domain. They have a better performance on images with weak boundaries. The Chan-Vese (CV) model, proposed by Chan and Vese [19], is one of the most popular region-based models, but it cannot work well for the images with intensity inhomogeneity because it assumes that the intensities of

* Correspondence to: East Campus of Soochow University, No. 50, Donghuan Road, Suzhou City 215021, Jiangsu Province, China
E-mail addresses: dingkeyan93@outlook.com (K. Ding), 21513001@zju.edu.cn (L. Xiao), wgr@suda.edu.cn (G. Weng).

http://dx.doi.org/10.1016/j.sigpro.2016.12.021
Received 9 July 2016; Received in revised form 9 November 2016; Accepted 19 December 2016
Available online 20 December 2016

image are statistically homogeneous. In order to segment images with intensity inhomogeneity, Chan and Vese [20] and Tsai et al. [21] proposed two similar models, which are often called piecewise smooth (PS) model. However, these methods have a low computational efficiency and the parameter settings are complex.

Li et al. [22] proposed an active contour model driven by region-scalable fitting (RSF) energy which is originally termed as the local binary fitting (LBF) model [23]. The RSF model introduces the intensity information of local region by a scale parameter. Thus, it can segment the images with intensity inhomogeneity precisely and efficiently. However, if the initial contour is set inappropriately, the RSF model tends to stuck in local minima due to the fact that energy functional is non-convex [29,30]. A reasonable large scale parameter can relatively reduce the dependence of the initial contour, but it will decrease the accuracy of segmentation especially when the phenomenon of intensity inhomogeneity is severe [22]. Therefore, an inappropriate initial contour can lead to reduce the efficiency of the segmentation greatly, and even cause the failure of segmentation. It has become a great challenge to find an efficient way to address the initialization problem in the RSF model. In addition, when the initial contour is largely far from the real boundaries of the objects, the RSF model is time consuming.

Wang et al. [26] proposed an active contour model which combines local and global intensity fitting (LGIF) energy in a variational level set framework, which means it integrates the advantages of the LBF model and the PC model to segment the images. The LGIF energy is defined by a linear combination of local intensity fitting (LIF) energy and global intensity fitting (GIF) energy. It can deal with intensity inhomogeneity and has a good robustness for initialization by properly choosing the value of w, which controls the weight of the LIF energy and the GIF energy. But for different images, it is difficult to accurately predict the value of w, and it often needs adjustment according to the degree of inhomogeneity. He et al. [27] proposed a weighted RSF model based on local entropy, where the weight is the value of local entropy derived from the gray level distribution of image. It allows more flexible initialization and stronger robustness to noise compared to the original RSF model. But the complexity of the algorithm increased because of introducing the local entropy, and the problem of arbitrary initialization has not been solved. Bhadauria et al. [28] presented an active contour model which integrates spatial fuzzy c-mean (FCM) algorithm with the RSF model. The basic idea is using the results of FCM clustering to initialize the active contour automatically. It is easy to cause the error of segmentation when the clustering results of FCM are not good. Considering that the energy functional of most active contour models are non-convex, Chan et al. [29] proposed a method of transforming non-convex function into convex function. Hence it can overcome the drawback of sticking in local minima naturally, but the process of implementation is complicated. Yang et al. [30] use global convex segmentation method and Split Bregman method to minimize the RSF energy. As a result, the segmentation efficiency is improved.

In this paper, we propose an improved active contour model based on region-scalable fitting (RSF) energy and optimized Laplacian of Gaussian (LoG) energy, which is insensitive to initialization and has a high efficiency for image segmentation. We first present a LoG energy term optimized by an energy functional which can smooth the homogeneous regions and enhance edge information at the same time. Then, we combine the LoG energy and the RSF energy in a variational level set framework. In addition, we add a distance regularized term to free the process of re-initialization, and a length term to eliminate the excess contours. Finally, the steepest descent method is used to minimize the entire energy functional. Compared with other major region-based models, our proposed model not only enhances the robustness of initialization, but also improves the efficiency and achieves an accurate segmentation result.

The remainder of this paper is organized as follows. Section 2 briefly reviews the CV model and the RSF model, and analyzes the drawback of RSF model. Section 3 introduces the proposed model. Section 4 shows some experimental results of synthetic and real images, and make a comparison with other region-based models. Section 5 presents some discussions about the proposed model. Last, Section 6 summarizes this paper.

2. Background

2.1. The CV model

Chan and Vese [19] proposed an active contour model based on the Mumford-Shah model [31]. Let I: $\Omega \rightarrow R$ be an input image and C be a closed curve, the energy functional is defined as follows:

$$E^{CV}(C, c_1, c_2) = \lambda_1 \int_{out(C)} |I(x) - c_1|^2 dx + \lambda_2 \int_{in(C)} |I(x) - c_2|^2 dx + u \cdot length(C) \tag{1}$$

where, λ_2, λ_1, u are positive constants. $I(x)$ is the intensity value on the point x. c_1 and c_2 are two constants that approximate the image intensities inside and outside the contour C, respectively. The data terms (the first and second terms) drive curve to approach the boundaries of object, and the Euclidean length term (the third term) is used to regularize the contour. Only when the contour C is located at the boundaries of the object can the energy E^{CV} reach the minimum value. Because c_1 and c_2 are involved in the global properties of the image intensity, the segmentation results will be wrong if the image intensities inside or outside the contour are inhomogeneous.

2.2. The RSF model

Li et al. [22,23] proposed an active contour model based on region-scalable fitting (RSF) energy in order to segment images with intensity inhomogeneity. The core idea of the RSF model is to define a local intensity fitting energy by introducing a kernel function, that is

$$E^{RSF}(C, f_1, f_2) = \lambda_1 \int_\Omega \left(\int_{out(C)} K_\sigma(x - y) |I(y) - f_1(x)|^2 dy \right) dx + \lambda_2 \int_\Omega \left(\int_{in(C)} K_\sigma(x - y) |I(y) - f_2(x)|^2 dy \right) dx \tag{2}$$

where K_σ is a Gaussian kernel and the standard deviation is σ. f_1 and f_2 are two smooth functions that approximate the intensities of image outside and inside the contour C in a local region, respectively. This energy in Eq. (2) can be represented by a level set formulation, and then the energy minimization problem can be converted to solving a level set evolution equation.

The curve is represented by the zero level set of a Lipschitz function ϕ expressed in Eq. (3), which takes positive values outside the contour and negative values inside the contour, respectively.

$$\begin{cases} \phi(x) < 0, x \in inside(C) \\ \phi(x) = 0, x \in C \\ \phi(x) > 0, x \in outside(C) \end{cases} \tag{3}$$

Accordingly, the energy functional E^{RSF} in Eq. (2) can be rewritten as follows:

$$E^{RSF}(\phi, f_1, f_2) = \lambda_1 \int_\Omega \left(\int_\Omega K_\sigma(x - y) |I(y) - f_1(x)|^2 H_\varepsilon(\phi) dy \right) dx + \lambda_2 \int_\Omega \left(\int_\Omega K_\sigma(x - y) |I(y) - f_2(x)|^2 (1 - H_\varepsilon(\phi)) dy \right) dx \tag{4}$$

where $H_\varepsilon(\phi)$ is the regularized Heaviside function approximated by a smooth function defined in Eq. (5). Its derivative is the regularized Dirac function defined in Eq. (6).

$$H_\varepsilon(x) = \frac{1}{2}\left(1 + \frac{2}{\pi}\arctan\left(\frac{x}{\varepsilon}\right)\right) \tag{5}$$

$$\delta_\varepsilon(x) = \frac{\varepsilon}{\pi(\varepsilon^2 + x^2)} \tag{6}$$

In addition, a length term $L(\phi)$ is added to smooth the contour in

the RSF model, and a distance regularization term $P(\phi)$ is included to preserve the regularity of the level set function, which can keep a stable level set evolution and free the procedure of re-initialization [16]. Therefore, the entire energy functional can be expressed as follows:

$$I^{RSF}(\phi, f_1, f_2) = E^{RSF}(\phi, f_1, f_2) + \upsilon L(\phi) + \mu P(\phi) \tag{7}$$

where

$$L(\phi) = \int \delta(\phi)|\nabla\phi(x)|dx \tag{8}$$

$$P(\phi) = \int \frac{1}{2}(|\nabla\phi(x)| - 1)^2 dx. \tag{9}$$

Minimizing the above energy functional in Eq. (7) by using the steepest descent method, the following variational formulations can be obtained:

$$\frac{\partial\phi}{\partial t} = -\delta_\varepsilon(\phi)(\lambda_1 e_1 - \lambda_2 e_2) + \nu\delta_\varepsilon(\phi) div\left(\frac{\nabla\phi}{|\nabla\phi|}\right) + \mu\left(\nabla^2\phi - div\left(\frac{\nabla\phi}{|\nabla\phi|}\right)\right) \tag{10}$$

where $e_1(x)$ and $e_2(x)$ are

$$\begin{cases} e_1(x) = \int_\Omega K_\sigma(y - x)|I(x) - f_1(y)|^2 dy \\ e_2(x) = \int_\Omega K_\sigma(y - x)|I(x) - f_2(y)|^2 dy \end{cases} \tag{11}$$

with

$$\begin{cases} f_1(x) = \frac{\int_\Omega K_\sigma(x-y)[H_\varepsilon(\phi(y))\cdot I(y)]dy}{\int_\Omega K_\sigma(x-y)H_\varepsilon(\phi(y)dy} \\ f_2(x) = \frac{\int_\Omega K_\sigma(x-y)[(1-H_\varepsilon(\phi(y))\cdot I(y)]dy}{\int_\Omega K_\sigma(x-y)[1-H_\varepsilon(\phi(x)]dy} \end{cases} \tag{12}$$

The standard deviation σ of the kernel function plays an important role in practical applications. It can be seen as a scale parameter that controls the size of local region. Because the localization property of the Gaussian kernel function, the contribution of the intensity $I(y)$ is decreased to zero when the point y far away the center point x. Hence, the RSF energy is dominated by the intensity of point y in a neighborhood of x. Meanwhile, the value of f_1 and f_2 in Eq. (12) can be seen as the weighted averages of the image intensities in a Gaussian window outside and inside the contour, respectively. This is why the RSF model can achieve the accurate segmentation for images with intensity inhomogeneity.

2.3. The drawback of the RSF model

Theoretically, we had known that the RSF model can handle the images with intensity inhomogeneity effectively. However, if the initial contour set inappropriately, the speed of curve evolution may reduce sharply and the curve C will be stuck in local minima finally. That means, the different positions of initial contour may cause the different segmentation results, and an inappropriate initial contour can cause the failure of the segmentation. This can be demonstrated by a simple experiment about segmenting a synthetic image with intensity inhomogeneity, as shown in Fig. 1. The setting of parameters is same to [22]. We can know from Fig. 1(a) that the evolution curve accurately located at the boundaries of the object after 200 iterations. But in Fig. 1(b)–(d), some curves stuck in the middle of both background and foreground regions after 1000 iterations. Thus, the segmentation results are wrong. Note that the time required for segmentation is related to the position of the initial contour. The initial contour closer to the boundaries of object, the less iterations needed, and vice versa.

3. The proposed model

In this section, an energy functional based on optimized LoG of image is proposed and combined with the RSF energy to overcome the drawbacks of the original RSF model.

LoG operator is a famous second-order differential operator edge detection operator. The principle is that the image I is first smoothed by the Gaussian filter, and then using Laplacian operator to detect the edge of this image. The mathematical definition of LoG is

$$\Delta(G_\sigma * I) = \left[\frac{\partial^2 G_\sigma(x, y)}{\partial x^2} + \frac{\partial^2 G_\sigma(x, y)}{\partial y^2}\right] * I(x, y) \tag{13}$$

where $G_\sigma(x, y)$ a Gaussian kernel function with standard deviation σ. The LoG of image is negative on the bright side and positive on the dark side, as shown in Fig. 2. The positions of zero-crossing are the regions where the gray value jumped. Therefore, the location of the edge can be obtained by detecting the zero-crossings of the second-order difference of the image.

However, the LoG of image is very sensitive to the change of intensity due to the existence of second-order derivative. It means many points of zero-crossing are false edge points, which is mainly caused by intensity inhomogeneity or noise. In order to optimize the LoG of image, namely smooth the homogeneous regions and enhance the edge of object, we propose an energy functional as follows:

$$E^{LoG}(L) = \iint_\Omega g(|\nabla I|) \times (L - 0)^2 + (1 - g(|\nabla I|)) \times (L - \beta \times \Delta(G_\sigma * I))^2 dxdy \tag{14}$$

where L represents the value of optimized LoG of image, and $g(|\nabla I|) = e^{-\alpha|\nabla G_\sigma * I|}$, α, β are positive constants. $g(|\nabla I|)$ is a edge indictor. The values of $g(|\nabla I|)$ are small and approximately equal to 0 at the locations near the object boundaries. And the values of $g(|\nabla I|)$ are large and approximately equal to 1 in the homogeneous regions. $(L - 0)^2$ is the data fitting term that measures the proximity between the optimized LoG and zero plane. When energy is descending, the term $g(|\nabla I|) \times (L - 0)^2$ will drive L close to 0 in the homogeneous regions. Thus, it is helpful to smooth the homogeneous regions. Similarly, $(L - \beta \times \Delta(G_\sigma * I))^2$ is the data fitting term that measures the proximity between the optimized LoG and the original LoG of image. The term $(1 - g(|\nabla I|)) \times (L - \beta \times \Delta(G_\sigma * I))^2$ will drive L close to $\Delta(G_\sigma * I)$ at the locations near the object boundaries. Thus, it can preserve the object edges when β is equal to 1. And when β is larger than 1, it can enhance the object edges.

By minimizing the energy in Eq. (14), the following Euler-Lagrange equation can be obtained:

$$g(|\nabla I|) \times L - (1 - g(|\nabla I|)) \times (L - \beta \times \Delta(G_\sigma * I)) = 0 \tag{15}$$

And using steepest gradient descent method to solve Eq. (15), we can obtain the following iterative equation:

$$\frac{\partial L}{\partial t} = g(|\nabla I|) \times L - (1 - g(|\nabla I|)) \times (L - \beta \times \Delta(G_\sigma * I)) \tag{16}$$

The stable solution of Eq. (16) is the optimized LoG of image. Take a synthetic image showed in Fig. 3(a) for example, Fig. 3(b) and Fig. 3(c) show the original LoG and the optimized LoG of image after 100 iterations, respectively. The parameters σ=1, α=0.01, β=5 and Δt=0.01. In Fig. 3(d), the green line is the cross-section of the original LoG, and the red line is the optimized LoG in the same row. We can know from Fig. 3 that the image of optimized LoG is smoother in the homogeneous regions and steeper near the object boundaries compared to the original LoG.

Next, we propose the following energy functional expressed by variational level set formulation:

$$E^{OL}(\phi) = \omega L_\Delta(\phi) + \upsilon L(\phi) + \mu P(\phi) = \omega \iint_\Omega H(\phi) L(x, y) dxdy + \upsilon \iint_\Omega \delta(\phi)|\nabla\phi| dxdy + \mu \iint_\Omega (|\nabla\phi| - 1)^2 dxdy \tag{17}$$

The parameters ω, ν and μ are the weight coefficients of each term. The $L_\Delta(\phi)$ is optimized LoG term, where $L(x, y)$ is obtained by solving

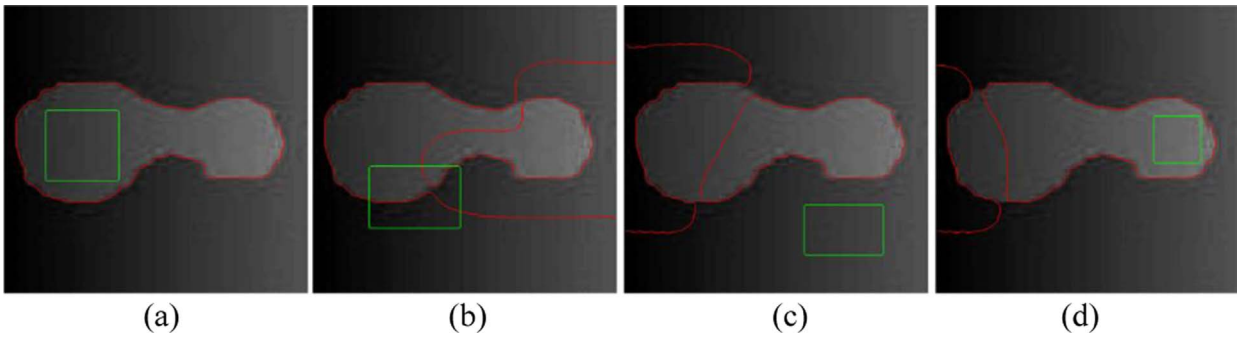

Fig. 1. Four segmentation results of synthetic image in RSF model with the different positions of initial contour. The green line is initial contour and the red line is final contour. (For interpretation of the references to color in this figure legend, the reader is referred to the web version of this article.)

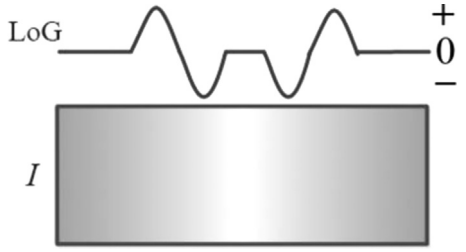

Fig. 2. The LoG of image.

Eq. (16). The function of $L(x, y)$ can detect the boundaries of objects quickly and accurately. It should be noticed that $L_\Delta(\phi)$ is different from the following Laplacian energy functional in Eq. (18) proposed by Kimmel and Bruckstein [32]. We use optimized LoG function $L(x, y)$ to replace the Laplacian of image $\Delta I(x, y)$.

$$L(\phi) = \iint_\Omega \Delta I(x, y) H(\phi) dxdy \tag{18}$$

In addition, we add the length term $L(\phi)$ defined in Eq. (8) to eliminate the excess contours and the distance regularized term $P(\phi)$ defined in Eq. (9) to free the procedure of re-initialization.

Though minimizing $E^{OL}(\phi)$ in Eq.(17), all the boundaries of objects can be detected quickly. However, considering that LoG operator is a global detection method, some false edges will still be included in the final results even though the optimization has been carried out, especially when segmenting the images with weak edges and severely inhomogeneous backgrounds. A relatively large weight of $L(\phi)$ can reduce this excess contours, but it will cause the leakage of edge at the same time. It will be proved in Section 4.

Thus, we combine the optimized LoG energy with the RSF energy as follows:

$$E^{RSFSL} = E^{RSF}(\phi, f_1, f_2) + E^{OL}(\phi) \tag{19}$$

where $E^{RSF}(\phi, f_1, f_2)$ is the RSF energy defined in Eq. (4), which makes use of local region information to drive the curve approach the target boundaries. $E^{OL}(\phi)$ is the optimized LoG energy defined in Eq. (17), which makes use of optimized LoG to detect the boundaries. Using the steepest descent method to minimize the above energy functional in Eq. (19), the following gradient flow equation can be obtained:

$$\frac{\partial \phi}{\partial t} = -\delta_\varepsilon(\phi)(\lambda_1 e_1 - \lambda_2 e_2) + \omega \delta_\varepsilon(\phi) \times L + \nu \delta_\varepsilon(\phi) div\left(\frac{\nabla \phi}{|\nabla \phi|}\right) + \mu\left(\Delta \phi - div\left(\frac{\nabla \phi}{|\nabla \phi|}\right)\right) \tag{20}$$

where $e_1(x)$ and $e_2(x)$ are the same to Eq. (11). Eq. (20) is the level set evolution equation to be solved in the proposed model.

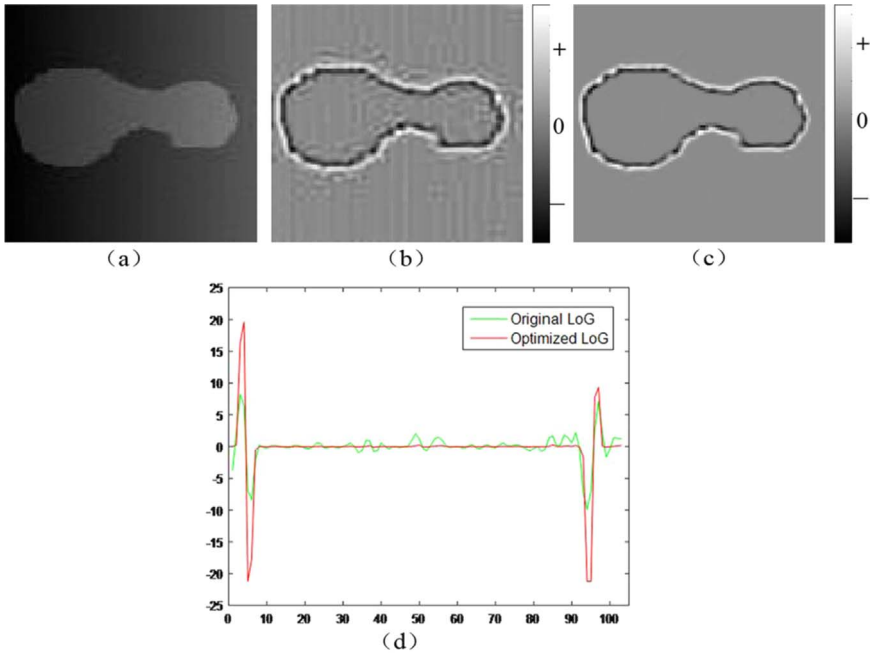

Fig. 3. Comparison between the original LoG and the optimized LoG for a synthetic image. (a) Original image. (b) The original LoG. (c) The optimized LoG. (d) The cross-section of the original LoG and the optimized LoG in the middle row. (For interpretation of the references to color in this figure, the reader is referred to the web version of this article.)

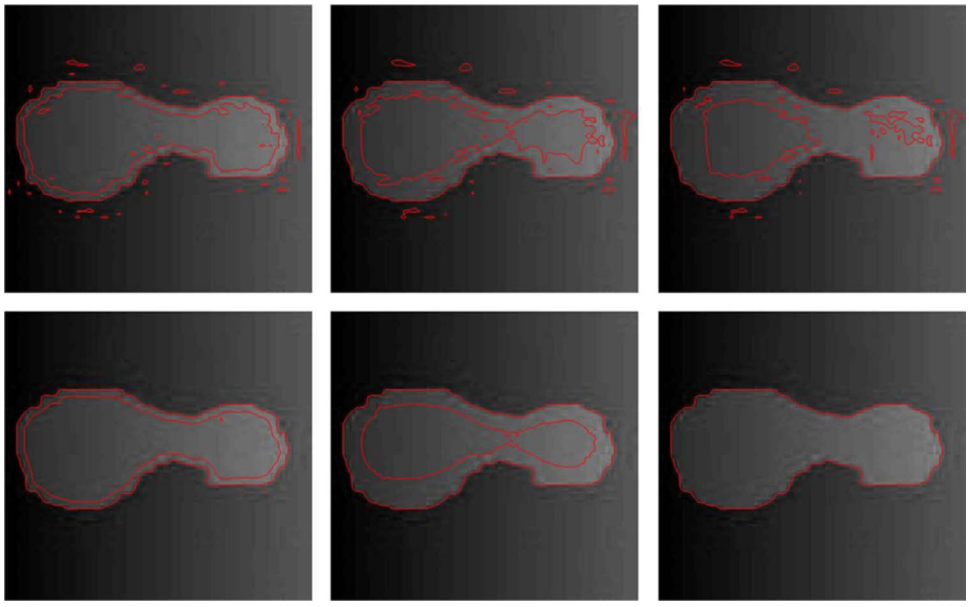

Fig. 4. Comparison between the segmentation result of the original LoG and the optimized LoG. Upper and lower rows are the process of curve evolution with original LoG term and optimized LoG term, respectively. Column 1: 5 iterations. Column 2: 50 iterations. Column 3: 150 iterations.

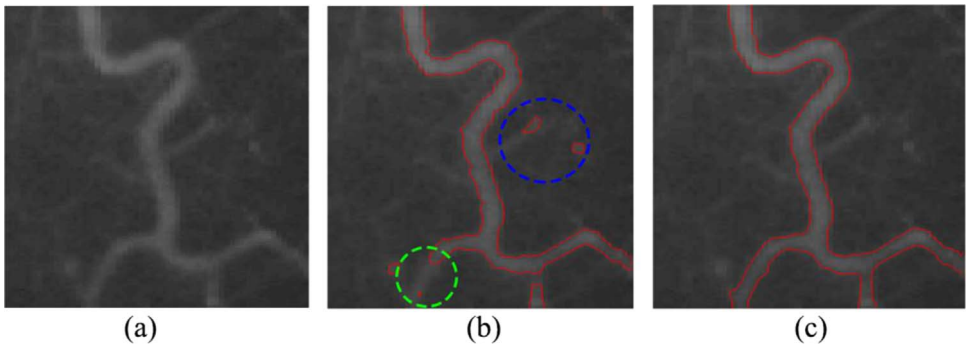

Fig. 5. The segmentation results for a real image. (a) Original vessel image. (b) The wrong segmentation result without the RSF energy. (d) The correct segmentation result with the RSF energy. (For interpretation of the references to color in this figure, the reader is referred to the web version of this article.)

4. Experimental results

In this section, the proposed model will be tested by some synthetic and real images, and the results will be compared with other major region-based models, especially the original RSF model. All the spatial partial derivatives $\frac{\partial\phi}{\partial x}$ and $\frac{\partial\phi}{\partial y}$ in Eq. (20) is discretized as central differences and the temporal derivative is discretized as a forward difference. The stopping criteria of curve evolution is $|\frac{S_{i+2}-S_i}{S}| < 10^{-5}$. S represents the total area of image. S_i represents the area surrounded by the contour at the time i. Unless otherwise specified, we use the following parameters in the proposed model: σ=3, μ=2, υ=0.002×255^2, ω=10, λ_1=λ_2=1 and time step Δt=0.1. In the process of optimizing LoG, the parameters σ=1, α=0.01, β=5, Δt=0.01 and the number of iterations is 100. The proposed model is implemented in Matlab R2014a on a 2.6-GHz Inter(R) Core(TM) i5 personal computer.

We first analyze the segmentation results without the RSF energy and make a comparison between the original LoG term and the optimized LoG term. The initial level set function ϕ_0 is initialized as a constant function whose value is 1. Upper and lower rows of Fig. 4 show the process of curve evolution with original LoG term and optimized LoG term, respectively. Fig. 4 shows that the original LoG term generates many trivial contours and the segmentation time is longer. Therefore, using optimized LoG to replace original LoG is helpful to get a correct segmentation result more quickly and precisely. We will use the optimized LoG term in the following examples.

For some images, using the optimized LoG energy alone is not enough for correct segmentation. For example, we choose a real vesssel image whose edge is weak and the background is severely inhomogeneous, as shown in Fig. 5(a). Fig. 5(b) shows the corresponding segmentation result. There are some excess contours (i.e. green dotted circle in Fig. 5(b)) and the phenomenon of edge leakage (i.e. blue dotted circle in Fig. 5(b)). Thus, no matter how to adjust the parameter υ, it cannot get a correct segmentation result. We add the RSF energy and make it plays a dominant role in the proposed model. The weight of LoG term is dropped to 5 and the weight of length term υ is set to 0.001×255^2. Thus, a correct segmentation is obtained, as shown in Fig. 5(c).

Next, we will show the segmentation results of the proposed model for some real images in Fig. 6. The process of curve evolution from the initial contour to the final contour is shown in every row of Fig. 6 for the corresponding images. The image in the first row is a real vessel image with intensity inhomogeneity. The image in the second row is a coronary angiography image with quite weak edges. The image in the third row is a tubal angiography image with quite low contrast. The image in the fourth row is an image with nonuniform illumination and high level noises. In this experiment, the weight of length term υ is increased to 0.005×255^2 and the weight of optimized LoG term ω is changed to −10. The image in the fifth row is a cerebral angiography image with complex structures. In this experiment, υ=0.001×255^2 and ω=−10. The image in the sixth row is an image of bacteria under a microscope. In this experiment, υ=0.010×255^2 and ω=5. The image in

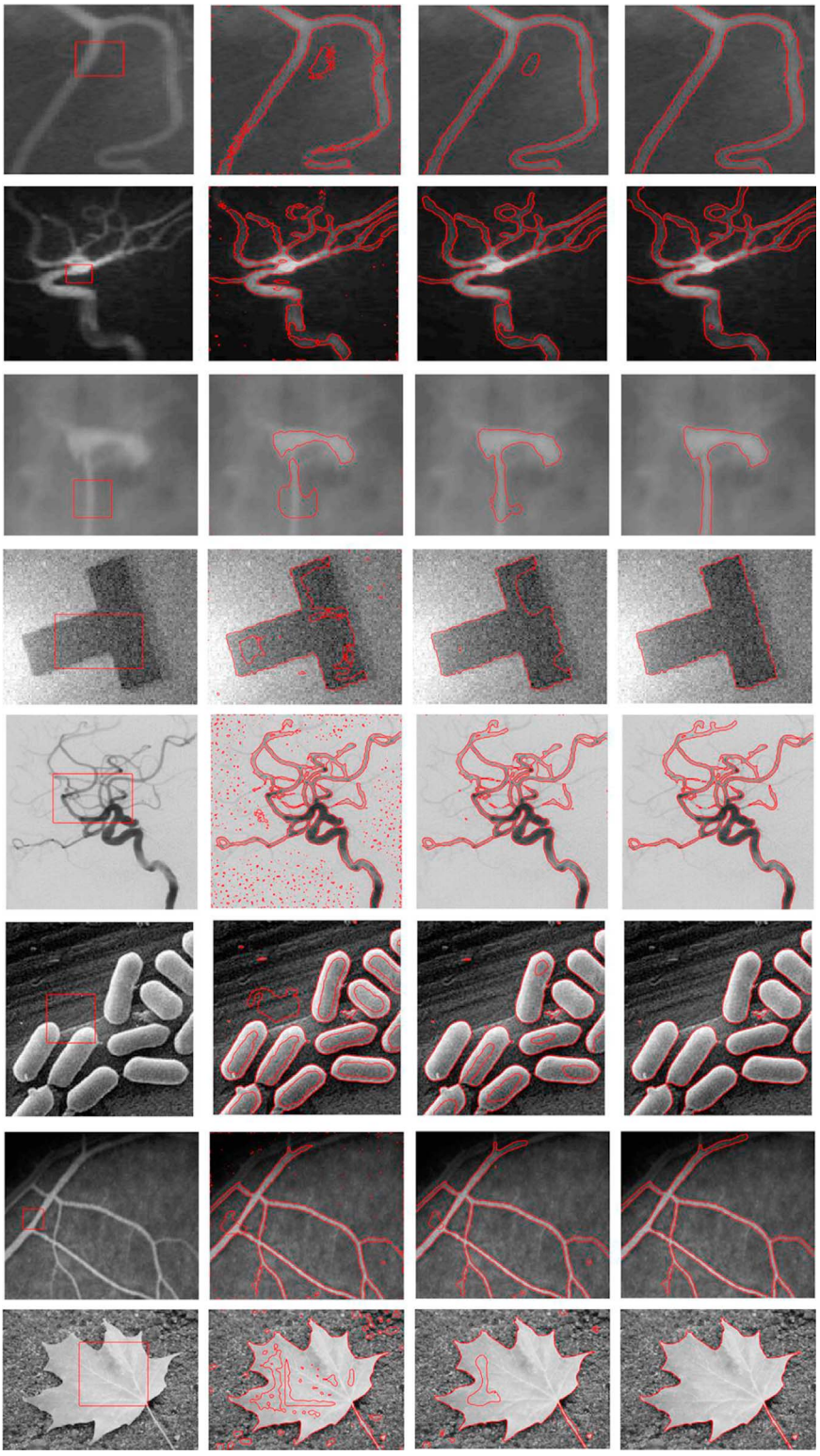

Fig. 6. Segmentation results of the proposed method for some real images. Every row represents the process of curve evolution from the initial contour (in the left-most column) to the final contour (in the right-most column).

the seventh row is a stem leaf image with inhomogeneous backgrounds. The image in the last row is a leaf image with noisy backgrounds. The right-most column of Fig. 6 shows that the desired segmentation results have been obtained for these images by using our model.

Then, we will analyze the importance of optimized LoG term by comparing the proposed model with the original RSF model. The initial level set function ϕ_0 is initialized as a binary step function which takes a negative constant value −1 inside zero level set and a positive constant value 1 outside. Unless otherwise specified, the parameters of the RSF model are the same to the proposed model. Take the images in the first row, third row and fifth row of Fig. 6 for examples, we set four different positions of initial contour in each image. Figs. 7–9 show the segmentation results of the original RSF model and the proposed model in upper row and lower row, respectively. The green line is initial

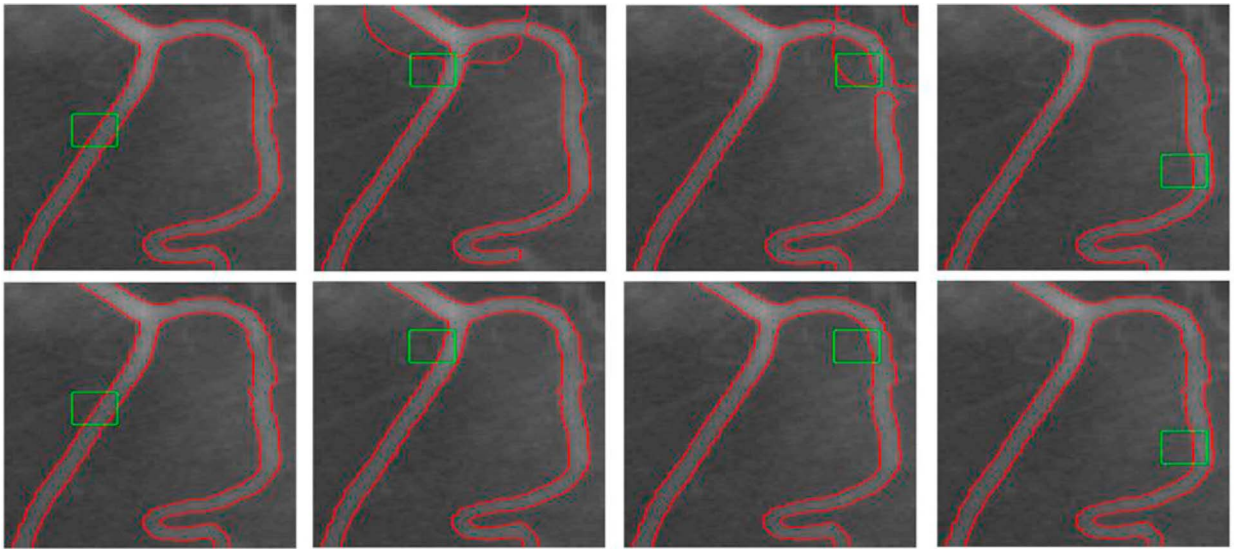

Fig. 7. Comparisons between the RSF model and the proposed model with different initial contours for a vessel image. Upper row: final results of the RSF model. Lower row: final results of the proposed model. (For interpretation of the references to color in this figure, the reader is referred to the web version of this article.)

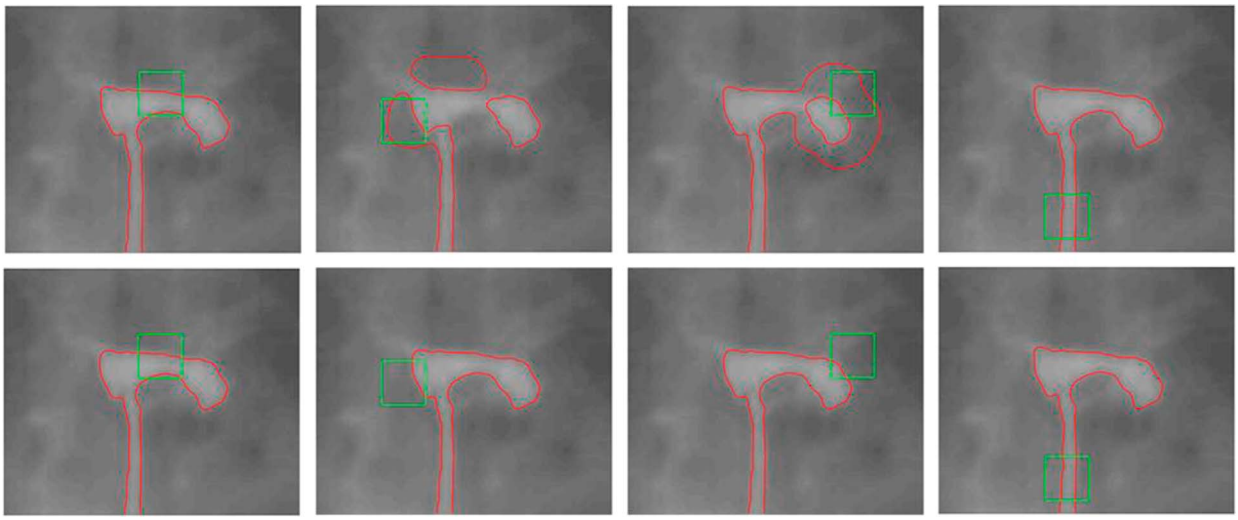

Fig. 8. Comparisons between the RSF model and the proposed model with different initial contours for a tubal angiography image. Upper row: final results of the RSF model. Lower row: final results of the proposed model. (For interpretation of the references to color in this figure, the reader is referred to the web version of this article.)

contour and the red line is final contour.

From Fig. 7, we notice that only the first and last cases of initial contour get the correct segmentation results in the RSF model. But in the proposed model, each case of initial contour obtains the correct results. Similarly, Fig. 8 shows that the first and last cases of initial contour get the correct segmentation results in the RSF model. But in the proposed model, each case of initial contour obtains the desired results. Fig. 9 shows that only the first case of initial contour gets the correct segmentation result in the RSF model. In the proposed model, each case of initial contour obtains the satisfactory results.

The above three examples show that the change of the initial contour has no effect on the segmentation results in our model. But in the RSF model, the change of the initial contour may cause a wrong segmentation result. In order to obtain a correct result, some parameters, such as the weight of length term and the scale parameter, must to be adjusted in the RSF model. Obviously, this is a cumbersome process. But in the proposed model, the correct segmentation results can be obtained without changing other parameters. Therefore, the proposed model is insensitive to the positions of initial contour, which means the addition of optimized LoG term can effectively solve the problem of sensitivity to initialization in the original RSF model.

Moreover, the addition of optimized LoG term can improve the segmentation efficiency greatly. Table 1 shows the corresponding number of iterations and time spent of Figs. 7–9. Note, we only list the segmentation time and the number of iterations under the first case of initial contour. From Table 1, we notice that both the number of iterations and time spent of the proposed model are the least. It means the proposed model has a higher segmentation efficiency than the RSF model for these images.

Finally, we will analyze the segmentation accuracy and efficiency of the proposed model by comparing with the famous CV model, RSF model and LGIF model [26]. These images in Fig. 10 come from Weizmann database [33]. From first row to last row of Fig. 10 show the initial contour, the ground-truth result, the segmentation results of the CV model, the RSF model, the LGIF model and the proposed model, respectively. We use the dice similarity coefficient (DSC) to quantitatively evaluate the performances of these models [34]. DSC is defined as follows:

$$DSC = \frac{2(S_1 \cap S_2)}{S_1 + S_2} \tag{21}$$

where S_1 and S_2 represent a given baseline object region and the object region found by the model, respectively. The more the value of DSC close to 1, the higher the accuracy of segmentation.

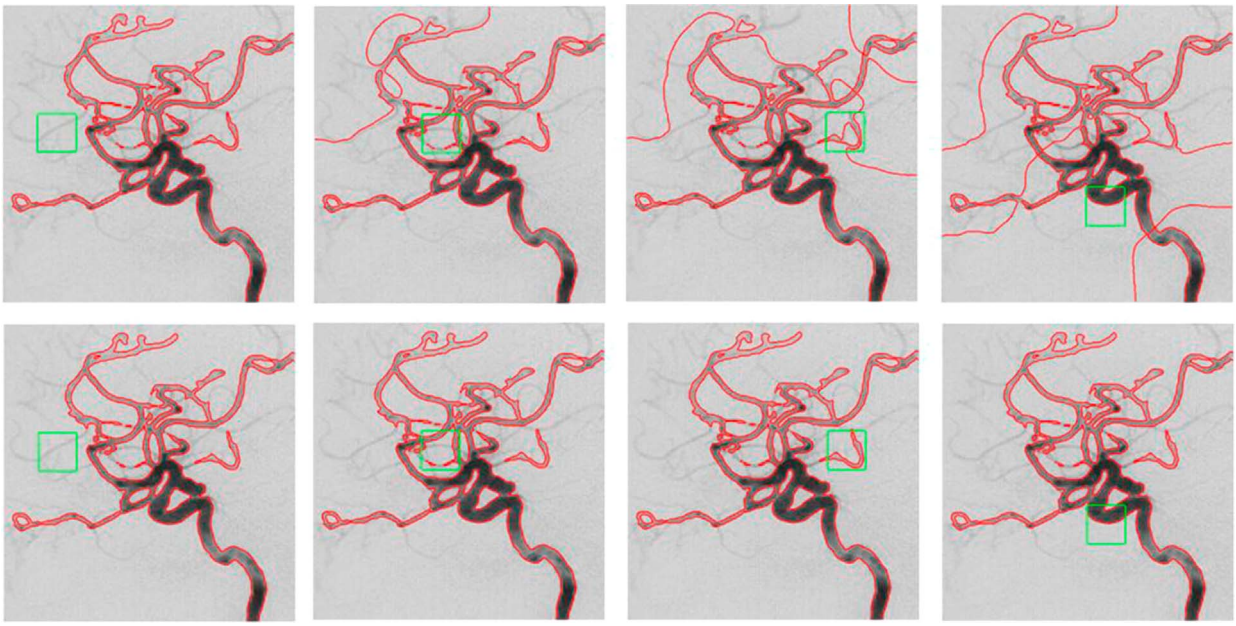

Fig. 9. Comparisons between the RSF model and the proposed model with different initial contours for a cerebral angiography image. Upper row: final results of the RSF model. Lower row: final results of the proposed model. (For interpretation of the references to color in this figure, the reader is referred to the web version of this article.)

Table 1
The number of iterations and time spent of Figs. 7–9 in the RSF model and the proposed model.

Image (Pixels)	The RSF model Iterations time (s)	The proposed model Iterations time (s)
Fig. 6 (100×96)	182 1.543	38 0.325
Fig. 7 (108×90)	80 0.772	56 0.443
Fig. 8 (150×150)	312 2.886	64 0.621

Table 2 shows the dice similarity coefficient and the time spent of the CV model, the RSF model, the LGIF model and the proposed model. From Table 2, we can know that the value of DSC of our model is the highest among these models although it is not much higher than the other models. The segmentation time of the proposed model is less than the RSF model and the LGIF model, and more than the CV model sometimes. But the segmentation results of the CV model are not accurate enough or even wrong for some images. Generally, the performance of the proposed model is better than the CV model, the RSF model and the LGIF model.

5. Discussions

5.1. About the edge detection operator

There are many differential operators for edge detection. Common edge detection operators including Roberts operator, Sobel operator, Prewitt operator, Canny operator, Laplacian operator, LoG operator and Difference of Gaussian (DoG) operator, *etc.* They have been widely used in image processing and pattern recognition [35,36].

In this paper, only the second-order differential operators based on the zero crossing point can be applied to the proposed model, such as Laplacian operator, LoG operator and DoG operator. And the first-order differential operators, such as Roberts operator, Sobel operator and Prewitt operator, are infeasible in our model. In other word, the operator used in the proposed model should satisfy the following conditions: one side of the edge is positive, the other side is negative, and the middle of edge is zero. Obviously, Laplacian operator, LoG operator and DoG operator are applicable. In this paper, we use LoG operator as the part of the proposed model. DoG operator is also feasible because LoG can be approximated as the difference between the two Gaussian functions, namely DoG. Thus, using DoG to substitute LoG can get almost same results in most cases.

5.2. About the optimization of LoG

The optimization of LoG plays an important role in the proposed model. First, it should be emphasized that the process of optimization is fast, which spends only about 0.02 s when the iteration number is 100. Hence, the time spent on optimization is negligible. In the process of optimization, the function $g(|\nabla I|) = e^{-\alpha|\nabla G_\sigma * I|}$ is a key point because it determines which area needs to be smoothed or sharpened. The parameter α has an impact on the function $g(|\nabla I|)$. The general range of α is 0.01–0.05. A small value of α will enhance the effect of smoothness, and vice versa. Take the image in Fig. 5 for an example, Fig. 11 shows the image of optimized LoG with the change of α. For images with weak edges and severe intensity inhomogeneity, α should be set to a relatively large value, otherwise the real edges of objects will be smoothed.

5.3. About the weight of LoG term ω

The parameter ω is a constant, which controls the weight of the optimized LoG energy in the proposed model. The general range of ω is 5–15 for most images. When the edge of object is weak, the ω should be set to a relatively large value. It should be noticed that the value of ω has a good robustness. Take the image in Fig. 7 for an example, the correct segmentation result can be obtained when the value of ω=5, 10 or 15, and the time spent is almost same. Of additional note, ω can take a negative value. When ω is negative, for images with bright target and dark background, such as Fig. 7, the curve will be evolved along the outer boundary of object due to the property of LoG operator. But for images with dark target and light background, such as Fig. 9, the curve will be evolved along the inner boundary of object. In most cases, the desired segmentation results can be obtained more quickly when the curve evolves along the inner boundary, especially for images with small objects.

5.4. About the application scope of the proposed model

The proposed model is applicable only for two-phase image. Thus,

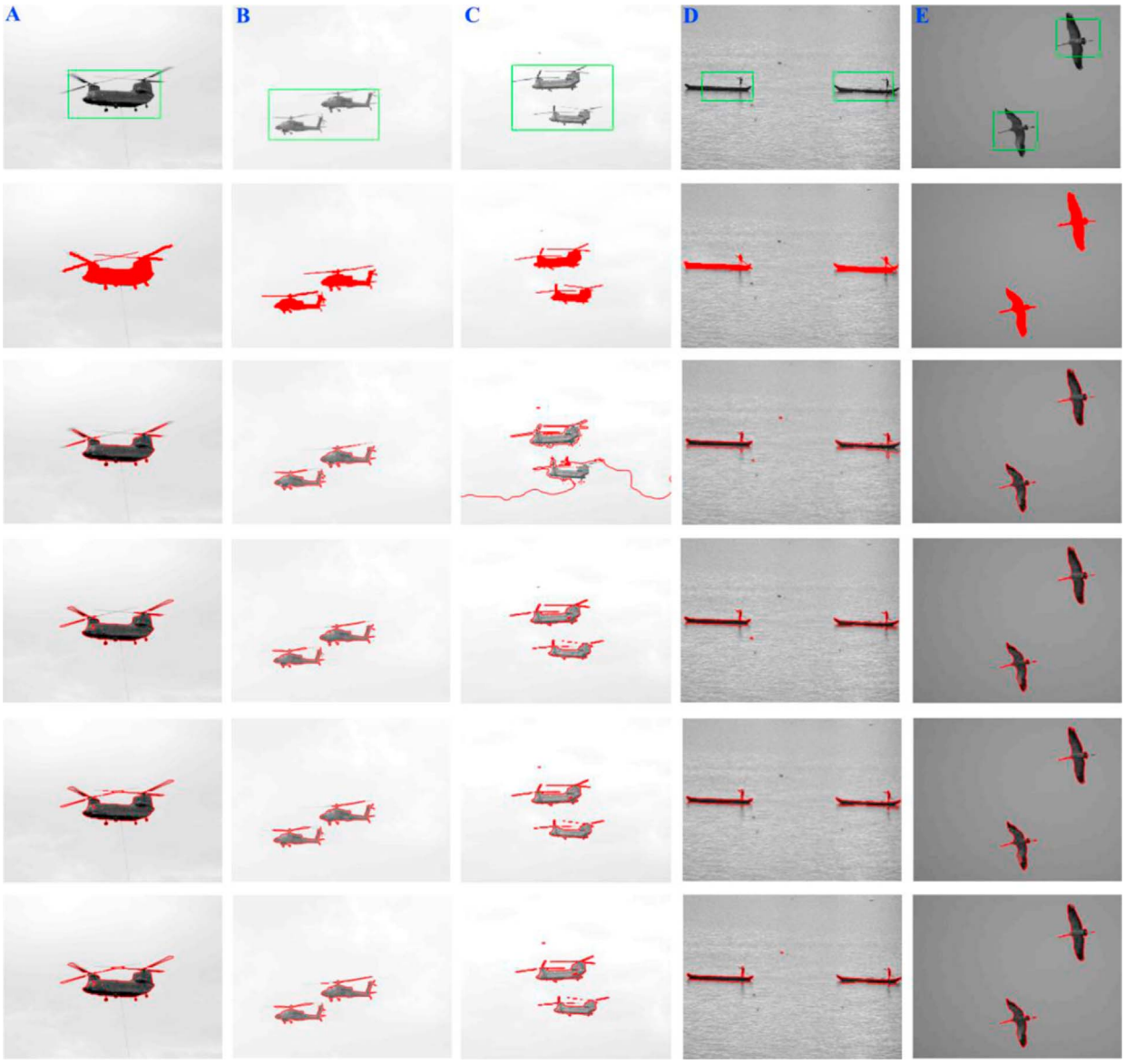

Fig. 10. Segmentation results of the CV model, the RSF model, the LGIF model and the proposed model. First row: the initial contour. Second row: the ground-truth. Third row: the CV model. Fourth row: the RSF model. Fifth row: the LGIF model. Last row: the proposed model.

Table 2
The dice similarity coefficient and the segmentation time of the CV model, the RSF model, the LGIF model and the proposed model. (DSC/Time(s)).

Image	CV	RSF	LGIF	**Our**
A (300×225)	0.9045/0.985	0.9121/2.833	0.9202/1.743	**0.9241/1.459**
B (300×232)	0.8734/2.161	0.9020/4.345	0.9012/2.712	**0.9183/1.743**
C (300×225)	0.3331/2.263	0.9251/3.261	0.9270/2.015	**0.9278/1.255**
D (300×207)	0.8438/2.060	0.9214/3.981	0.9302/2.518	**0.9321/2.048**
E (300×248)	0.9192/1.160	0.9029/3.253	0.9101/2.310	**0.9356/1.203**

the proposed model cannot work well for the object with obvious multiple colors. For example, Fig. 12 shows the undesirable segmentation results of the proposed model. This is because the objects in these images have significantly different values of intensity. We will consider solving this problem by exploiting the multi-phase segmentation in the future.

6. Conclusions

In this paper, we have presented an active contour model which combines region-scalable fitting and optimized LoG energy for image segmentation, where the LoG term is optimized by an energy functional, which can smooth the homogeneous regions and enhance edge information. Compared with the original RSF model, the proposed model not only enhances the robustness of initialization, but also improves the efficiency and achieves an accurate segmentation result. In addition, the process of optimization can be applied to the edge stopping function which often used in edge-based active contour models.

Acknowledgements

The authors would like to thank the anonymous reviewers for valuable comments to improve this paper and Dr. Chunming Li for sharing the code of the RSF model in website: http://www.engr.uconn.edu/cmli/. Besides, this work is supported by the National Nature Science Foundation of China [grant number 61473201].

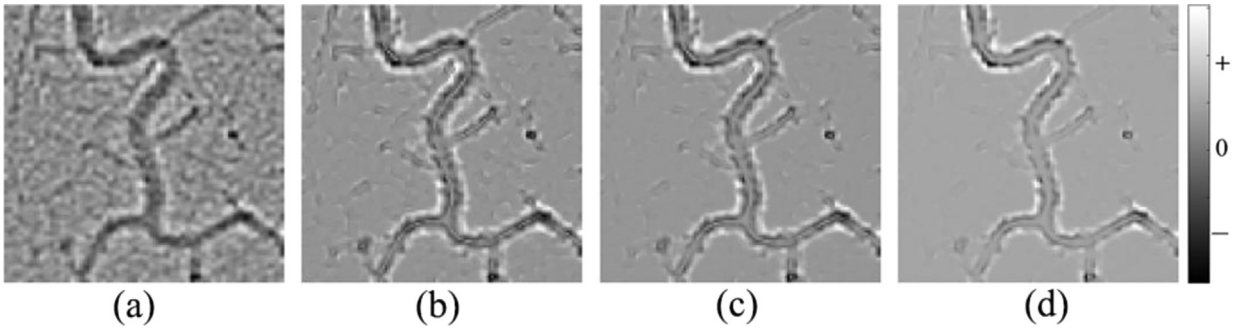

Fig. 11. The image of optimized LoG with the change of α. (a) Original LoG. (b) Optimized LoG with α=0.10. (c) Optimized LoG with α=0.05. (d) Optimized LoG with α=0.01.

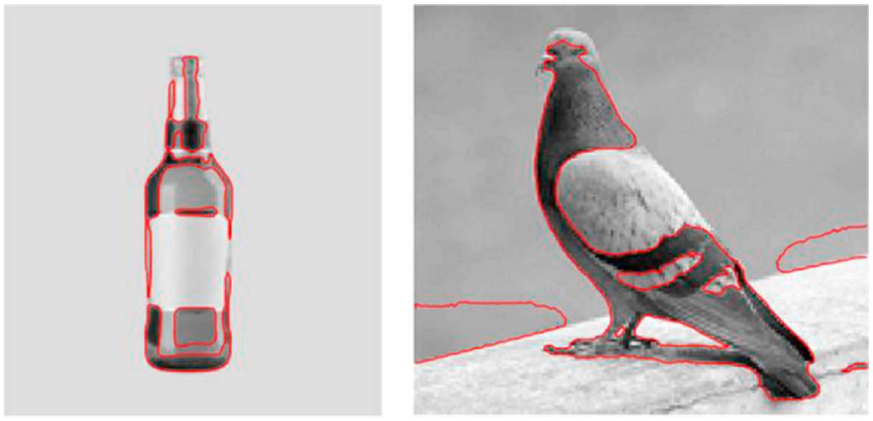

Fig. 12. Examples of undesirable segmentation results in the proposed model.

References

[1] Q. Chen, L. Zhao, J. Lu, G. Kuang, N. Wang, Y. Jiang, Modified two-dimensional Otsu image segmentation algorithm and fast realization, IET Image Process. 6 (4) (2012) 426–433.

[2] M. Rafe, Elliptic theory of differential edge operators, Commun. Part. Diff. Eq. 16 (10) (1991) 1615–1664.

[3] S.A. Hojjatoleslami, J. Kittler, Region growing: a new approach, IEEE Trans. Image Process. 7 (7) (1998) 1079–1084.

[4] M. Kass, A. Witkin, D. Terzopoulos, Snakes: active contour models, Int. J. Comput. Vis. 1 (4) (1988) 321–331.

[5] H. Fu, C. Wang, D. Tao, M.J. Black, Occlusion boundary detection via deep exploration of context, in: Proceedings of IEEE Conference on Computer Vision and Pattern Recognition (CVPR), 2016, pp. 241–250.

[6] M.E. Sargin, L. Bertelli, B.S. Manjunath, K. Rose, Probabilistic occlusion boundary detection on spatio- temporal lattices, in: Proceedings of the IEEE International Conference on Computer Vision (ICCV), 2009, pp. 560–567.

[7] T.F. Cootes, C.J. Taylor, Active shape models, Proc. Br. Mach. Vis. Conf. (1995) 266–275.

[8] T.F. Cootes, G.J. Edwards, C.J. Taylor, Active appearance models, IEEE Trans. Pattern Anal. Mach. Intell. 23 (6) (1998) 681–685.

[9] J. Sung, T. Kanade, D. Kim, A Unified gradient-based approach for Combining ASM into AAM, Int. J. Comput. Vis. 75 (2) (2006) 353–362.

[10] C. Ding, C. Xu, D. Tao, Multi-task pose-invariant face recognition, IEEE Trans. Image Process. 24 (3) (2015) 980–993.

[11] S.J. Osher, R.P. Fedkiw, The level set methods and dynamic Implicit surfaces, Appl. Mech. Rev. 57 (3) (2004) B15.

[12] V. Caselles, F. Catte, T. Coll, F. Dibos, A geometric model for active contours in image processing, Numer. Math. 66 (1) (1993) 1–31.

[13] V. Caselles, R. Kimmel, G. Sapiro, Geodesic active contours, Int. J. Comput. Vis. 22 (1) (1997) 61–79.

[14] N. Paragios, R. Deriche, Geodesic active contours and level sets for the detection and tracking of moving objects, IEEE Trans. Pattern Anal. Mach. Intell. 22 (3) (2000) 266–280.

[15] N. Paragios, R. Deriche, Geodesic active regions and level set methods for supervised texture segmentation, Int. J. Comput. Vis. 46 (3) (2002) 223–247.

[16] C. Li, C. Xu, C. Gui, M.D. Fox, Distance regularized level set evolution and its application to image segmentation, IEEE Trans. Image Process. 19 (12) (2010) 3243–3254.

[17] Q. Li, T. Deng, W. Xie, Active contours driven by divergence of gradient vector flow, Signal Process. 120 (2016) 185–199.

[18] R. Ronfard, Region-based strategies for active contour models, Int. J. Comput. Vis. 13 (2) (1994) 229–251.

[19] T. Chan, L. Vese, Active contours without edges, IEEE Trans. Image Process. 10 (2) (2001) 266–277.

[20] L. Vese, T. Chan, A multiphase level set framework for image segmentation using the Mumford–Shah model, Int. J. Comput. Vis. 50 (3) (2002) 271–293.

[21] A. Tsai, A. Yezzi, A.S. Willsky, Curve evolution implementation of the Mumford-Shah functional for image segmentation, denoising, interpolation, and magnification, IEEE Trans. Image Process. 10 (8) (2001) 1169–1186.

[22] C. Li, C. Kao, J. Gore, Z. Ding, Minimization of region-scalable fitting energy for image segmentation, IEEE Trans. Image Process. 17 (10) (2008) 1940–1949.

[23] C. Li, C. Kao, J. Gore, Z. Ding, Implicit active contours driven by local binary fitting energy, in: Proceedings of the IEEE Conference on Computer Vision and Pattern Recognition (CVPR), 2007, pp. 1–7.

[24] K. Zhang, H. Song, L. Zhang, Active contours driven by local image fitting energy, Pattern Recogn. 43 (4) (2010) 1199–1206.

[25] L. Wang, L. He, A. Mishra, C. Li, Active contours driven by local Gaussian distribution fitting energy, Signal Process. 89 (12) (2009) 2435–2447.

[26] L. Wang, C. Li, Q. Sun, D. Xia, C. Kao, Active contours driven by local and global intensity fitting energy with application to brain MR image segmentation, Comput. Med. Imag. Grap. 33 (7) (2009) 20520–20531.

[27] C. He, Y. Wang, Q. Chen, Active contours driven by weighted region-scalable fitting energy based on local entropy, Signal Process. 92 (2) (2012) 587–600.

[28] H. Bhadauria, M. Dewal, Intracranial hemorrhage detection using spatial fuzzy c-mean and region-based active contour on brain CT imaging, Signal Image Video P. 8 (2) (2014) 357–364.

[29] T. Chan, S. Esedoglu, M. Nikolova, Algorithms for finding global minimizers of image segmentation and denoising models, SIAM J. Appl. Math. 66 (5) (2006) 1632–1648.

[30] Y. Yang, C. Li, C.Y. Kao, S. Osher, Split bregman method for minimization of region-scalable fitting energy for image segmentation, in: Proceedings of the International Symposium on Visual Computing, 2010, pp. 117–128.

[31] D. Mumford, J. Shah, Optimal approximation by piecewise smooth function and associated variational problems, Commun. Pure. Appl. Math. 42 (5) (1989) 577–685.

[32] R. Kimmel, A.M. Bruckstein, Regularized Laplacian zero crossings as optimal edge integrators, Int. J. Comput. Vis. 53 (3) (2003) 225–243.

[33] S. Alpert, M. Galun, R. Basri, A. Brandt, Image segmentation by probabilistic bottom-up aggregation and cue integration, in: Proceedings of the IEEE Conference on Computer Vision and Pattern Recognition (CVPR), 2007, pp. 1–8.

[34] L.R. Dice, Measures of the amount of ecologic association between species, Ecology 26 (3) (1945) 297–302.

[35] X. Tan, B. Triggs, Enhanced local texture feature sets for face recognition Under difficult lighting conditions, IEEE Trans. Image Process. 19 (6) (2010) 1635–1650.

[36] C. Ding, J. Choi, D. Tao, L.S. Davis, Multi-directional multi-level dual-cross patterns for robust face recognition, IEEE Trans. Pattern Anal. Mach. Intell. 38 (3) (2016) 518–531.